Aerial image based technique for measurement of lens aberrations up to 37th Zernike coefficient in lithographic tools under partial coherent illumination

Wei Liu[1], Shiyuan Liu[2,*], Tingting Zhou[1], and Lijuan Wang[1]

[1]*Wuhan National Laboratory for Optoelectronics, Huazhong University of Science and Technology, Wuhan 430074, China*

[2]*State Key Laboratory of Digital Manufacturing Equipment and Technology, Huazhong University of Science and Technology, Wuhan 430074, China*

shyliu@mail.hust.edu.cn

Abstract: This paper proposes a technique for in situ measurement of lens aberrations up to the 37th Zernike coefficient in lithographic tools under partial coherent illumination. The technique requires the acquisition and analysis of aerial image intensities of a set of 36 binary gratings with different pitches and orientations. By simplifying the theoretical derivation of the optical imaging under partial coherent illumination, two linear models are proposed in a compact expression with two matrixes, which can be easily obtained in advance by numerical calculation instead of by lithographic simulators, and then used to determine the Zernike coefficients of odd aberration and even aberration respectively. The simulation work conducted by PROLITH has validated the theoretical derivation and confirms that such a technique yields a superior quality of wavefront estimate with an accuracy of Zernike coefficients on the order of 0.1mλs (λ = 193nm) and an accuracy of wavefronts on the order of mλs, due to further considering the influence of the partial coherence factor on pupil sampling. It is fully expected that this technique will simple to implement and will provide a useful practical means for the in-line monitoring of imaging quality of lithographic tools under partial coherent illumination.

©2009 Optical Society of America

OCIS codes: (110.5220) Photolithography; (120.0120) Instrumentation, measurement, and metrology; (220.1010) Aberrations theory; (110.4980) Partial coherence in imaging

References and links

1. B. W. Smith, and R. Schlief, “Understanding lens aberration and influences to lithographic imaging,” Proc. SPIE **4000**, 294–306 (2000).
2. J. Sung, M. Pitchumani, and E. G. Johnson, “Aberration measurement of photolithographic lenses by use of hybrid diffractive photomasks,” Appl. Opt. **42**(11), 1987–1995 (2003).
3. F. Wang, X. Wang, and M. Ma, “Measurement technique for in situ characterizing aberrations of projection optics in lithographic tools,” Appl. Opt. **45**(24), 6086–6093 (2006).
4. H. Nomura, and T. Sato, “Techniques for measuring aberrations in lenses used in photolithography with printed patterns,” Appl. Opt. **38**(13), 2800–2807 (1999).
5. F. Zernike, “Beugungstheorie des Schneidenverfahrens und seiner verbesserten form, der Phasenkontrastmethode,” Physica **1**(7-12), 689–704 (1934).
6. M. Born, and E. Wolf, Principles of Optics, 7th edition, (Pergamon, 1999), chap. 9.
7. M. Ma, X. Wang, and F. Wang, “Aberration measurement of projection optics in lithographic tools based on two-beam interference theory,” Appl. Opt. **45**(32), 8200–8208 (2006).
8. L. Zavyalova, A. Bourov, and B. W. Smith, “Automated aberration extraction using phase wheel targets,” Proc. SPIE **5754**, 1728–1737 (2005).
9. M. van de Kerkhof, W. de Boeij, H. Kok, M. Silova, J. Baselmans, and M. Hemerik, “Full optical column characterization of DUV lithographic projection tools,” Proc. SPIE **5377**, 1960–1970 (2004).
10. T. Fujii, K. Suzuki, Y. Mizuno, and N. Kita, “Integrated projecting optics tester for inspection of immersion ArF scanner,” Proc. SPIE **6152**, 615237 (2006).

#111794 - $15.00 USD Received 22 May 2009; revised 31 Jul 2009; accepted 1 Oct 2009; published 9 Oct 2009

11. T. Fujii, J. Kougo, Y. Mizuno, H. Ooki, and M. Hamatani, "Portable phase measuring interferometer using Shack-Hartmann method," Proc. SPIE **5038**, 726–732 (2003).
12. Y. Ohsaki, T. Mori, S. Koga, M. Ando, K. Yamamoto, T. Tezuka, and Y. Shiode, "A new on-machine measurement system to measure wavefront aberrations of projection optics with hyper-NA," Proc. SPIE **6154**, 615424 (2006).
13. H. van der Laan, M. Dierichs, H. van Greevenbroek, E. McCoo, F. Stoffels, R. Pongers, and R. Willekers, "Aerial image measurement methods for fast aberration setup and illumination pupil verification," Proc. SPIE **4346**, 394–407 (2001).
14. Q. Yuan, X. Wang, Z. Qiu, F. Wang, M. Ma, and L. He, "Coma measurement of projection optics in lithographic tools based on relative image displacements at multiple illumination settings," Opt. Express **15**(24), 15878–15885 (2007).
15. Z. Qiu, X. Wang, Q. Yuan, and F. Wang, "Coma measurement by use of an alternating phase-shifting mask mark with a specific phase width," Appl. Opt. **48**(2), 261–269 (2009).
16. Q. Yuan, X. Wang, Z. Qiu, F. Wang, and M. Ma, "Even aberration measurement of lithographic projection system based on optimized phase-shifting marks," Microelectron. Eng. **86**(1), 78–82 (2009).
17. J. K. Tyminski, T. Hagiwara, N. Kondo, and H. Irihama, "Aerial image sensor: in-situ scanner aberration monitor," Proc. SPIE **6152**, 61523D (2006).
18. T. Hagiwara, N. Kondo, I. Hiroshi, K. Suzuki, and N. Magome, "Development of aerial image based aberration measurement technique," Proc. SPIE **5754**, 1659–1669 (2005).
19. H. Hopkins, "Canonical coordinates in geometrical and diffraction image theory," Jpn. J. Appl. Phys. **4**, 31–35 (1965).
20. H. Hopkins, "On the diffraction theory of optical images," Proc. R. Soc. A **217**(1130), 408–432 (1953).
21. T. Nakashima, S. D. Slonaker, T. Kudo, and S. Hirukawa, "Evaluation of Zernike sensitivity method for CD distribution," Proc. SPIE **5040**, 1600–1610 (2003).

1. Introduction

As the limit of optical lithography is pushed and feature densities continue to increase, lens aberration has become one of the most important factors to evaluate the imaging quality of lithographic tools [1–4]. One method to mathematically model lens aberrations utilizes Zernike polynomials, which are a complete orthogonal set of polynomials over the interior of the unit circle [5–7]. The Zernike series representation is useful as it provides explicit expressions for the well-known low order aberrations such as spherical, coma, astigmatism, etc., while higher-order polynomials are less significant in the description of aberrations. However, in order to meet the requirement of optical path tolerances on the order of several nanometers over extremely large aperture of current projection lens, the higher-order coefficients of Zernike polynomials are becoming increasingly more important for monitoring lens performance on a regular basis [8]. Therefore, there is a need for the manufacturers of lithographic tools to develop in situ techniques and systems to accurately measure aberrations up to the 37th or even higher-order Zernike coefficient.

Generally, in situ measurement techniques can be roughly classified into two categories: one is pupil based and the other is image based. In recent years, a variety of pupil based techniques for in situ aberration measurement have been reported, including ILIAS (integrated lens interferometer at scanner) [9], iPot (integrated projecting optics tester) [10,11], and iPMI (in situ phase measurement interferometer) [12]. Although capable of fast and accurately retrieving aberrations up to the 37th Zernike coefficient, these techniques are concluded to in situ PMI (phase measurement interferometer) method, thus integrated with complex apparatus such as embedded interferometer and micro lens array which result in high cost for lithographic tools.

Due to the advantage of lower cost and easier implement in tools without a portable PMI, aerial image based techniques have been widely used for in situ measurement of lens aberrations. ASML Corporation has developed an aerial image based technique known as TAMIS (TIS at multiple illumination settings), which utilizes a TIS (transmission image sensor) built into the wafer stage for receiving the aerial image intensity of the test binary mark [13]. Using the image displacements of the mark at multiple numerical aperture (NA) and partial coherence settings, the Zernike coefficients can be calculated with a matrix of sensitivities which is a function of NA/σ under multiple illumination settings. Wang et al recently reported a series of TAMIS based techniques to improve the measurement accuracy of coma and even aberrations by optimization of the test marks using phase-shifting gratings [14–16]. Although TAMIS and its improved techniques are robustness and speed, the

#111794 - $15.00 USD Received 22 May 2009; revised 31 Jul 2009; accepted 1 Oct 2009; published 9 Oct 2009
(C) 2009 OSA

accuracy is fully dependent upon the matrix of sensitivities, which should be carefully obtained in advance and can be only calculated by lithographic simulators. Moreover, the test marks used in TAMIS based techniques are orientated in 0° and 90° or additional directions of 45° and 135°, which maintain high sensitivity only to spherical, coma and astigmatism, thus are unable to measure high-order aberrations up to the 37th Zernike coefficient. In the meantime, Nikon Corporation has proposed a Z37 AIS (Aerial Image Sensor) technique which is able to measure aberrations up to the 37th Zernike coefficient by introducing a set of 36 binary grating marks with different pitches and orientations [17,18]. As these gratings are corresponding to 72 pupil sampling points, the wavefront aberration at each sampling point over the pupil plane can be easily obtained by the spectrum of the aerial image intensity. However, since obtaining the wavefront at each sampling point requires highly coherent illumination, the Z37 AIS technique works best with coherent sources, and is therefore unsuitable for aberration measurement in conventional lithographic tools under partial coherent illumination.

In this paper, by making improvements of both TAMIS and Z37 AIS techniques, we propose what we believe to be a novel technique for in situ measurement of lens aberrations up to the 37th Zernike coefficient in lithographic tools under partial coherent illumination. The technique utilizes the aerial image intensities of a set of 36 binary gratings with different pitches and orientations. The optical property of the + 1st-order spectrum of the aerial image intensity is investigated based on the Hopkins theory of partially coherent imaging. By simplifying the theoretical derivation of the optical imaging under partial coherent illumination, two linear models are proposed in a compact expression with two matrixes, which can be easily obtained in advance by numerical calculation instead of by lithographic simulators and then are used to determine the Zernike coefficients of odd aberration and even aberration respectively. The overall performance of the proposed technique was subsequently simulated by the lithographic simulator PROLITH in order to demonstrate the validity and accuracy of the proposed technique for measuring aberrations up to the 37th Zernike coefficient.

2. Theory

2.1 Aerial image spectrum analysis

A schematic drawing of the optical lithographic imaging is shown in Fig. 1. In order to simplify the expressions of the imaging system, in the drawing on the left we introduce the Cartesian object plane coordinates (x_0, y_0), image plane coordinates (x_i, y_i) and pupil plane coordinates (f, g) which are all normalized according to canonical coordinates proposed by Hopkins [19], thus the cut off frequency from the pupil plane is normalized to the unit of one. In the drawing on the right, the orientation of the binary grating is defined by the angle θ ranging from 0° to 180°. Our technique utilizes a set of 36 binary grating objects orientated in θ = 0°, 30°, 45°, 90°, 120°, and 135° with different spatial periods. Consider the one-dimensional object in the θ direction with normalized spatial period $p_m = 1/\rho_m$ and opening width $p_m/2$, where m = 1, 2, 3, …, 36. The spectrum of the mth grating becomes:

$$O(\rho) = \frac{1}{2}\operatorname{sinc}\left(\frac{\rho}{2\rho_m}\right)\sum_{l=-\infty}^{+\infty}\delta\left(\rho - l\rho_m\right),\ l \in Z, \tag{1}$$

where ρ is the spatial frequency in the θ direction. As is seen from Eq. (1), the even-order diffraction lights of the binary grating are missing except the 0th-order diffraction light. The spectrum $O(\rho)$ is nonzero only at odd frequencies and zero frequency: $\rho = 0, \pm\rho_m, \pm 3\rho_m, \ldots, (2k+1)\rho_m, k \in \mathrm{N}$.

#111794 - $15.00 USD Received 22 May 2009; revised 31 Jul 2009; accepted 1 Oct 2009; published 9 Oct 2009
(C) 2009 OSA

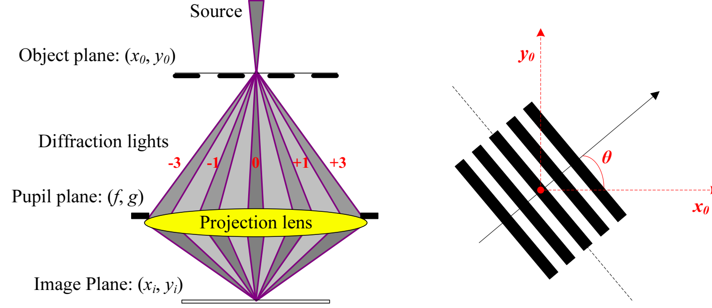

Fig. 1. Imaging of a binary grating object in a lithographic tool.

Similar to TAMIS and Z37 AIS, the proposed technique also utilizes an aerial image sensor built into the wafer stage for receiving the aerial image intensity of the test binary grating. The spectrum of the aerial image intensity is extracted by Fourier transformation and is subsequently analyzed for aberration measurement. Based on the scalar form of the Hopkins imaging theory [20], from Eq. (1) the + 1st-order spectrum of the aerial image intensity can be obtained only by the interaction of the 0th-order and + 1/-1st-order diffraction lights of the object [18], and can be expressed as:

$$I(\rho_m,\theta_m,\sigma,h)=\frac{1}{2\pi}\left[TCC\left(0,0;\alpha_m,\beta_m;\sigma,h\right)+TCC\left(-\alpha_m,-\beta_m;0,0;\sigma,h\right)\right], \quad (2)$$

where σ is the partial coherence factor, and defined as the effective source filling factor in the projection optics pupil [13,18]. The smaller the partial coherence factor is, the higher the degree of illumination coherence is. h is the axial shift of the aerial image sensor at the image plane (in nm). (α_m, β_m) express normalized Cartesian coordinates in the pupil plane corresponding to polar ones (ρ_m, θ_m):

$$\alpha_m=\rho_m\cos\theta_m,\ \ \beta_m=\rho_m\sin\theta_m\ . \quad (3)$$

TCC is introduced as the concept of transmission cross-coefficient:

$$TCC\left(f',g';f'',g'';\sigma,h\right)=\int\int_{-\infty}^{+\infty}J\left(f_c,g_c,\sigma\right)H\left(f'+f_c,g'+g_c,h\right)H^*\left(f''+f_c,g''+g_c,h\right)df_c dg_c\ . \quad (4)$$

Here, $J(f_c, g_c, \sigma)$ represents the effective source which is the image of the typical illumination source in the pupil plane:

$$J\left(f_c,g_c,\sigma\right)=\frac{1}{\pi\sigma^2}\mathrm{circ}\left(\frac{\sqrt{f_c^2+g_c^2}}{\sigma}\right). \quad (5)$$

The pupil function $H(f, g, h)$ represents the transmission function in the pupil plane and can be written as:

$$H\left(f,g,h\right)=\exp\left[-jkW\left(f,g,h\right)\right]\mathrm{circ}\left(\sqrt{f^2+g^2}\right), \quad (6)$$

where $k = 2\pi/\lambda$ is the wave number, λ is the wavelength of the monochromatic light source, and $W(f, g, h)$ is the total aberrated wavefront including the lens aberration $W_{lens}(f, g)$ that is commonly classified into an odd aberration $W_{odd}(f, g)$ and an even aberration $W_{even}(f, g)$, and another even-type aberration $W_{defocus}(f, g, h)$ that is induced by and proportional to the axial shift h of the aerial image sensor [21]:

$$W(f,g,h)=W_{lens}\left(f,g\right)+W_{defocus}\left(f,g,h\right), \quad (7)$$

#111794 - $15.00 USD Received 22 May 2009; revised 31 Jul 2009; accepted 1 Oct 2009; published 9 Oct 2009
(C) 2009 OSA

$$W_{lens}(f,g) = W_{odd}(f,g) + W_{even}(f,g), \tag{8}$$

$$W_{defocus}(f,g,h) = h \cdot w_{defocus}(f,g) = h\left[\sqrt{1 - NA^2\left(f^2 + g^2\right)} - 1\right], \tag{9}$$

where NA is the image-side numerical aperture of the projection lens.

2.2 Aberration measurement under partial coherent illumination

From Eq. (2), one method to measure aberrations up to Z_{37} term is Z37 AIS technique which is able to directly extract lens aberration $W_{lens}(\rho_m, \theta_m)$ at pupil sampling point (ρ_m, θ_m) [17,18]. However, as the partial coherence factor σ increases, there is no longer sampling point but sampling spot with a radius of σ, hence the lens aberration at each pupil sampling point is impossible to be accurately obtained. Therefore, the Z37 AIS technique should be improved by further considering the influence of partial coherence factor on pupil sampling.

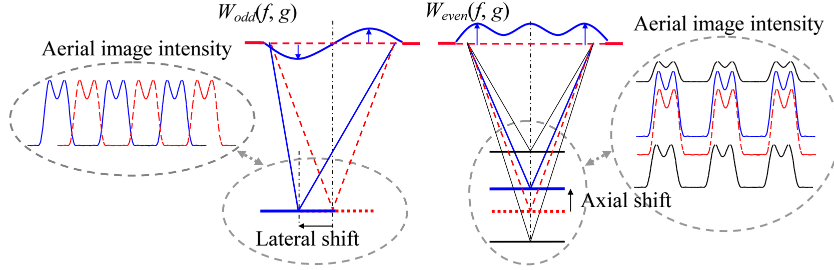

Fig. 2. The impact of aberrations on imaging.

As shown in Fig. 2, the impact of aberrations on imaging is the interaction of the phase shift and amplitude change of the spectrum of image intensity in frequency domain respectively caused by odd aberration and even aberration. From Eq. (2), the phase shift $\varphi(\rho_m,\theta_m,\sigma,h)$ and amplitude $\left|I(\rho_m,\theta_m,\sigma,h)\right|$ of the + 1st-order spectrum of aerial image intensity are given by:

$$\varphi(\rho_m,\theta_m,\sigma,h) = \arctan\left(\frac{\mathrm{Im}\left[I(\rho_m,\theta_m,\sigma,h)\right]}{\mathrm{Re}\left[I(\rho_m,\theta_m,\sigma,h)\right]}\right), \tag{10}$$

$$\left|I(\rho_m,\theta_m,\sigma,h)\right| = \sqrt{\mathrm{Re}^2\left[I(\rho_m,\theta_m,\sigma,h)\right] + \mathrm{Im}^2\left[I(\rho_m,\theta_m,\sigma,h)\right]}. \tag{11}$$

Here, the real part $\mathrm{Re}[I(\rho_m, \theta_m, \sigma, h)]$ and the imaginary part $\mathrm{Im}[I(\rho_m, \theta_m, \sigma, h)]$ are respectively written as:

$$\begin{aligned}\mathrm{Re}\left[I(\rho_m,\theta_m,\sigma,h)\right] = \frac{1}{(\pi\sigma)^2}\iint_{S(\sigma)} &\cos\left\{k\left[W_{odd}(\alpha_m+f_c,\beta_m+g_c) - W_{odd}(f_c,g_c)\right]\right\} \\ &\times\cos\left\{k\left[W_{even}(\alpha_m+f_c,\beta_m+g_c) - W_{even}(f_c,g_c)\right.\right. \\ &\left.\left.+h\cdot w_{defocus}(\alpha_m+f_c,\beta_m+g_c) - h\cdot w_{defocus}(f_c,g_c)\right]\right\} df_c dg_c\end{aligned}, \tag{12}$$

$$\begin{aligned}\mathrm{Im}\left[I(\rho_m,\theta_m,\sigma,h)\right] = \frac{1}{(\pi\sigma)^2}\iint_{S(\sigma)} &\sin\left\{k\left[W_{odd}(\alpha_m+f_c,\beta_m+g_c) - W_{odd}(f_c,g_c)\right]\right\} \\ &\times\cos\left\{k\left[W_{even}(\alpha_m+f_c,\beta_m+g_c) - W_{even}(f_c,g_c)\right.\right. \\ &\left.\left.+h\cdot w_{defocus}(\alpha_m+f_c,\beta_m+g_c) - h\cdot w_{defocus}(f_c,g_c)\right]\right\} df_c dg_c\end{aligned}, \tag{13}$$

#111794 - $15.00 USD Received 22 May 2009; revised 31 Jul 2009; accepted 1 Oct 2009; published 9 Oct 2009
(C) 2009 OSA

where the integral region $S(\sigma)$ is a intersection part of the two circles according to the circ functions in Eqs. (5) and (6), and is represented in Cartesian coordinates (f_c, g_c) as a shaded area shown in Fig. 3.

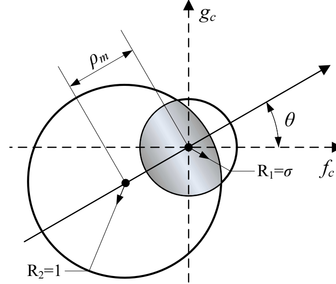

Fig. 3. Representation of the integral region S(σ).

Consider a small amount of aberrations in the projection lens:

$$W\left(f,g,h\right)\sim 0, \cos\left[kW\left(f,g,h\right)\right]\sim 1, \tan\left[kW\left(f,g,h\right)\right]\sim \sin\left[kW\left(f,g,h\right)\right]\sim kW\left(f,g,h\right). \quad (14)$$

Substituting Eq. (14) into Eq. (10), the expression of phase shift of the + 1st-order spectrum at the ideal focal plane corresponding to $h = 0$ can be simplified as:

$$\varphi\left(\rho_m,\theta_m,\sigma\right)=k\iint_{S(\sigma)}\left[W_{odd}\left(\alpha_m+f_c,\beta_m+g_c\right)-W_{odd}\left(f_c,g_c\right)\right]df_c dg_c\,. \quad (15)$$

The amplitude of the + 1st-order spectrum reaches the extreme value occurring at $h = D(\rho_m, \theta_m, \sigma)$ satisfying the condition:

$$\frac{\partial\left|I(\rho_m,\theta_m,\sigma,h)\right|}{\partial h}=0\,. \quad (16)$$

Substituting Eq. (14) into Eq. (16), the expression of axial shift $D(\rho_m, \theta_m, \sigma)$ can be simplified as:

$$D(\rho_m,\theta_m,\sigma)=\frac{\begin{array}{c}\iint_{S(\sigma)}\left[W_{even}\left(\alpha_m+f_c,\beta_m+g_c\right)-W_{even}\left(f_c,g_c\right)\right]\\ \times\left[w_{defocus}\left(f_c,g_c\right)-w_{defocus}\left(\alpha_m+f_c,\beta_m+g_c\right)\right]df_c dg_c\end{array}}{\iint_{S(\sigma)}\left[w_{defocus}\left(f_c,g_c\right)-w_{defocus}\left(\alpha_m+f_c,\beta_m+g_c\right)\right]^2 df_c dg_c}\,. \quad (17)$$

More details for derivation of Eqs. (15) and (17) can be found in Appendix A and B respectively.

By expressing aberrations as a series of Zernike polynomials, Eqs. (15) and (17) can be written as:

$$\varphi\left(\rho_m,\theta_m,\sigma\right)=\sum_{n_odd}Z_{n_odd}F_{n_odd}\left(\rho_m,\theta_m,\sigma\right), \quad (18)$$

$$D\left(\rho_m,\theta_m,\sigma\right)=\sum_{n_even}Z_{n_even}G_{n_even}\left(\rho_m,\theta_m,\sigma\right), \quad (19)$$

where *n_odd* indicates Zernike index for odd aberration, *n_even* indicates Zernike index for even aberration, $F_{n_odd}(\rho_m, \theta_m, \sigma)$ and $G_{n_even}(\rho_m, \theta_m, \sigma)$ can be expressed by:

$$F_{n_odd}\left(\rho_m,\theta_m,\sigma\right)=k\iint_{S(\sigma)}\left[R_{n_odd}\left(\alpha_m+f_c,\beta_m+g_c\right)-R_{n_odd}\left(f_c,g_c\right)\right]df_c dg_c\,, \quad (20)$$

#111794 - $15.00 USD Received 22 May 2009; revised 31 Jul 2009; accepted 1 Oct 2009; published 9 Oct 2009
(C) 2009 OSA

$$G_{n_even}\left(\rho_m,\theta_m,\sigma\right)=\frac{\begin{array}{c}\iint\limits_{S(\sigma)}\left[R_{n_even}\left(\alpha_m+f_c,\beta_m+g_c\right)-R_{n_even}\left(f_c,g_c\right)\right]\\ \times\left[w_{defocus}\left(f_c,g_c\right)-w_{defocus}\left(\alpha_m+f_c,\beta_m+g_c\right)\right]df_c dg_c\end{array}}{\iint\limits_{S(\sigma)}\left[w_{defocus}\left(f_c,g_c\right)-w_{defocus}\left(\alpha_m+f_c,\beta_m+g_c\right)\right]^2 df_c dg_c}. \quad (21)$$

Here, the function $R_n(f, g)$ indicates the nth Zernike polynomial for normalized Cartesian coordinate (f, g) over the pupil plane.

With a set of 36 binary gratings, two sets of 36 linear equations can be obtained from Eqs. (18) and (19), and respectively with 18 unknowns to be extracted. Since there are more equations than unknowns, both two sets of equations become over-determined and can be solved by the least-square method. In matrix notation the two sets of equations become:

$$\begin{bmatrix}\varphi\left(\rho_1,\theta_1,\sigma\right)\\ \varphi\left(\rho_2,\theta_2,\sigma\right)\\ \vdots\\ \varphi\left(\rho_{36},\theta_{36},\sigma\right)\end{bmatrix}=\begin{bmatrix}F_2\left(\rho_1,\theta_1,\sigma\right) & F_3\left(\rho_1,\theta_1,\sigma\right) & \cdots & F_{35}\left(\rho_1,\theta_1,\sigma\right)\\ F_2\left(\rho_2,\theta_2,\sigma\right) & F_3\left(\rho_2,\theta_2,\sigma\right) & \cdots & F_{35}\left(\rho_2,\theta_2,\sigma\right)\\ \vdots & \vdots & \vdots & \vdots\\ F_2\left(\rho_{36},\theta_{36},\sigma\right) & F_3\left(\rho_{36},\theta_{36},\sigma\right) & \cdots & F_{35}\left(\rho_{36},\theta_{36},\sigma\right)\end{bmatrix}\begin{bmatrix}Z_2\\ Z_3\\ \vdots\\ Z_{35}\end{bmatrix}, \quad (22)$$

$$\begin{bmatrix}D\left(\rho_1,\theta_1,\sigma\right)\\ D\left(\rho_2,\theta_2,\sigma\right)\\ \vdots\\ D\left(\rho_{36},\theta_{36},\sigma\right)\end{bmatrix}=\begin{bmatrix}G_4\left(\rho_1,\theta_1,\sigma\right) & G_5\left(\rho_1,\theta_1,\sigma\right) & \cdots & G_{37}\left(\rho_1,\theta_1,\sigma\right)\\ G_4\left(\rho_2,\theta_2,\sigma\right) & G_5\left(\rho_2,\theta_2,\sigma\right) & \cdots & G_{37}\left(\rho_2,\theta_2,\sigma\right)\\ \vdots & \vdots & \vdots & \vdots\\ G_4\left(\rho_{36},\theta_{36},\sigma\right) & G_5\left(\rho_{36},\theta_{36},\sigma\right) & \cdots & G_{37}\left(\rho_{36},\theta_{36},\sigma\right)\end{bmatrix}\begin{bmatrix}Z_4\\ Z_5\\ \vdots\\ Z_{37}\end{bmatrix}. \quad (23)$$

In a more compact notation Eqs. (22) and (23) can be rewritten as:

$$\mathbf{\Phi}=\mathbf{F}\mathbf{Z}_{odd}\ , \quad (24)$$

$$\mathbf{D}=\mathbf{G}\mathbf{Z}_{even}\ , \quad (25)$$

where $\mathbf{\Phi}$ and $\mathbf{D}$ are vectors respectively containing the phase shifts and the axial shifts at the setting of 36 binary gratings; $\mathbf{Z}_{odd}$ and $\mathbf{Z}_{even}$ are unknown vectors to be measured, and respectively containing the Zernike coefficients for odd aberration and even aberration; $\mathbf{F}$ and $\mathbf{G}$ are two matrixes for measuring odd aberration and even aberration respectively.

From Eqs. (24) and (25), each of the matrixes $\mathbf{F}$ and $\mathbf{G}$ has a compact expression as a function of ρ/θ under a certain partial coherence factor σ. It is obvious that our technique can be applied in conventional lithographic tools under partial coherent illumination, hence overcomes the limitation of the highly coherence illumination in the Z37 AIS technique. Note also that, all of the TAMIS, the Z37 AIS and our technique use the aerial image sensor to extract lateral and axial measurements of the image, while both of the Z37 AIS and our technique require obtaining the Fourier decomposition of the image to analyze the changes of the spectrum caused by aberrations. Furthermore, the TAMIS based techniques need to use a lithographic simulator to calculate the aberration sensitivities, while the proposed matrixes of our technique can be numerically calculated in advance from the analytical derivation. Taking advantage of a set of 36 binary gratings with different pitches and orientations, our technique is capable of measuring high-order aberrations up to the Z_{37} term.

2.3 Estimate of Zernike errors by lateral and axial metrology errors

In the proposed technique, it is needed to extract lateral and axial measurements of the image. According to Eqs. (24) and (25), the lateral or axial metrology error of the lithographic tool has an impact on the errors in Zernike estimate:

#111794 - $15.00 USD Received 22 May 2009; revised 31 Jul 2009; accepted 1 Oct 2009; published 9 Oct 2009
(C) 2009 OSA

$$\Delta\mathbf{\Phi} = \mathbf{F}\Delta\mathbf{Z}_{odd} \ , \tag{26}$$

$$\Delta\mathbf{D} = \mathbf{G}\Delta\mathbf{Z}_{even} \ , \tag{27}$$

where $\Delta\mathbf{\Phi}$ and $\Delta\mathbf{D}$ are vectors respectively containing the phase shift errors and the axial metrology errors at the setting of 36 binary gratings; $\Delta\mathbf{Z}_{odd}$ and $\Delta\mathbf{Z}_{even}$ are error vectors of Zernike coefficients; and the phase shift error $\Delta\varphi_m$ corresponding to the mth grating can be determined by:

$$\Delta\varphi_m = \frac{2\pi}{T_m}\Delta x \ , \tag{28}$$

where T_m (in nm) is the image-side pitch of the mth grating, and Δx (in nm) is the lateral metrology error of the lithographic tool. If the error for lateral metrology is 1nm and the error for axial metrology is 5nm, the resultant errors of Zernike coefficients can be estimated from Eqs. (26) and (27), and thus illustrated in Fig. 4. It is noted that the resultant error of the Z_4 term reaches 4.35mλ while the absolute error of other terms is less than 1mλ. This overall result is satisfactory and the much larger error of the Z_4 term is due to the little dependence of the sensitivity values $G_4(\rho_m, \theta_m, \sigma)$ on the setting (ρ_m, θ_m). The similar observation has also been reported in the TAMIS technique [13].

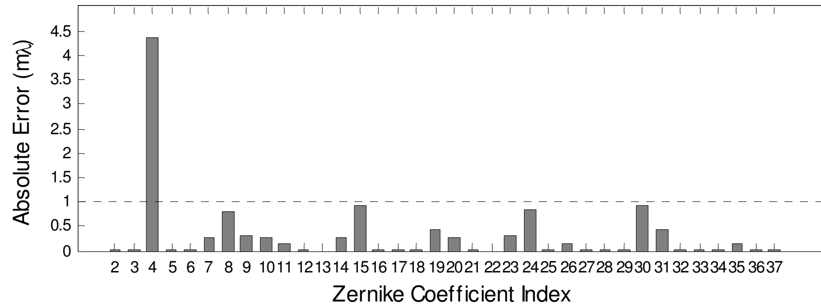

Fig. 4. Estimate of aberration errors with lateral metrology error of 1nm and axial metrology error of 5nm.

3. PROLITH simulation

The lithographic simulator PROLITH was used to simulate the overall measurement performance under partial coherence settings. The wavelength used in the simulation is 193nm and the NA is 0.75. Figure 5 shows the aberrated wavefront values with Zernike coefficients from Z_2 up to Z_{37} that we used as inputs for simulation.

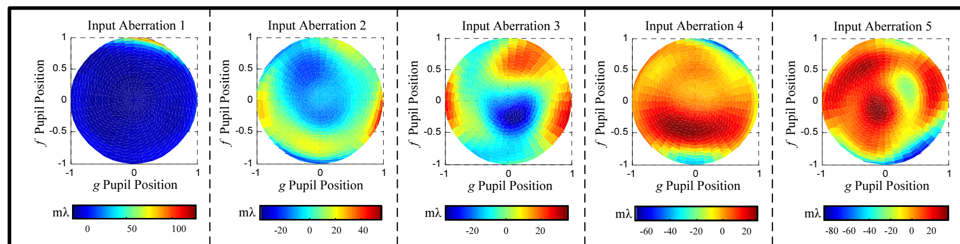

Fig. 5. Input values of aberrated wavefront for simulation.

#111794 - $15.00 USD Received 22 May 2009; revised 31 Jul 2009; accepted 1 Oct 2009; published 9 Oct 2009
(C) 2009 OSA

3.1 Validity of the theoretical derivation

The matrixes **F** and **G** obtained by numerical calculation are key factors for aberration measurement. The validity of the theoretical derivation of matrixes **F** and **G** can be proved by validating the linear models of Eqs. (24) and (25) using a typical partial coherence (e.g. σ = 0.31) for simulation. Figure 6 shows the correlation plots between the simulated shifts and the calculated shifts, by using all the input aberrated wavefronts shown in Fig. 5 for the simulation. Figure 6(a) represents the correlation plot between the simulated phase shifts obtained by the PROLITH and the predicted shifts calculated by Eq. (24), and Fig. 6(b) represents a correlation plot between the simulated axial shifts obtained by the PROLITH and the predicted shifts calculated by Eq. (25). Each of Fig. 6(a) and Fig. 6(b) contains 180 dots for 5 sets of 36 linear equations.

From the simulation results shown in Fig. 6 and lots of other simulation results under different highly partial coherences, it is observed that the maximum deviations of the phase shifts and axial shifts are on the order of 10^{-3}rads and nms, respectively. This excellent correlation demonstrates the validity of numerical calculation for matrixes **F** and **G**.

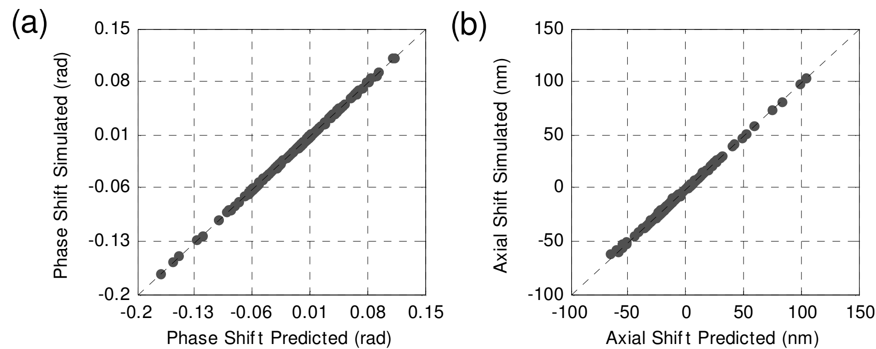

Fig. 6. Correlation plots between simulated and calculated shifts for all the input aberrated wavefronts under σ = 0.31. (a) Plot of predicted phase shifts versus simulated phase shifts. (b) Plot of predicted axial shifts versus simulated axial shifts. Each of (a) and (b) contains 180 dots corresponding to 5 sets of 36 linear equations.

3.2 Comparison with Z37 AIS technique

To verify the necessity of considering the influence of partial coherence on pupil sampling for the aberration measurement under partial coherent illumination, a comparison was performed with Z37 AIS technique by using the Input Aberration 1 shown in Fig. 5 as an input for the simulation.

Figure 7 shows the Root-Mean-Square (RMS) of the absolute measurement error of Zernike coefficients up to Z_{37}, by the simulation of Z37 AIS technique at multiple partial coherences from 0.01 to 0.4. From Fig. 7, it is clear that the RMS of measurement errors by Z37 AIS significantly increases as the partial coherence increases. As the partial coherence is smaller than 0.05 which represents a high degree of illumination coherence, the RMS value is less than 0.25mλ. However, as the partial coherence reaches 0.31, the RMS value increases to 3.6mλ which is an unacceptable error for the aberration measurement.

#111794 - $15.00 USD Received 22 May 2009; revised 31 Jul 2009; accepted 1 Oct 2009; published 9 Oct 2009
(C) 2009 OSA

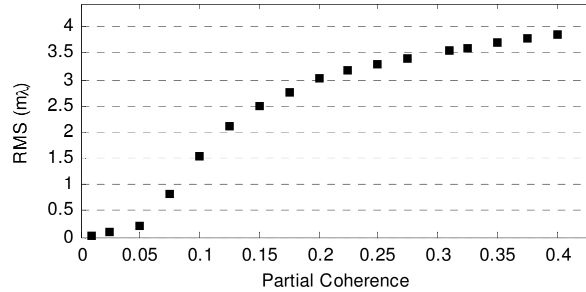

Fig. 7. Simulation result of Z37 AIS technique at multiple partial coherences for the Input Aberration 1.

Figure 8 shows the result of the proposed technique by the simulation with the partial coherence 0.31. The upper chart represents a comparison of the input Zernike coefficients and the measured values, and the lower chart represents the absolute errors of Zernike coefficients. The measured values of the Zernike coefficients are noted to coincide quite closely with the input values. From the simulation result, the absolute errors of all Zernike coefficients are less than 0.35mλ, and the RMS of the absolute errors of Zernike coefficients up to Z_{37} is 0.15mλ compared with 3.6mλ by Z37 AIS technique. It is clear that the measurement accuracy is greatly improved under partial coherent illumination, due to further considering the influence of partial coherence factor.

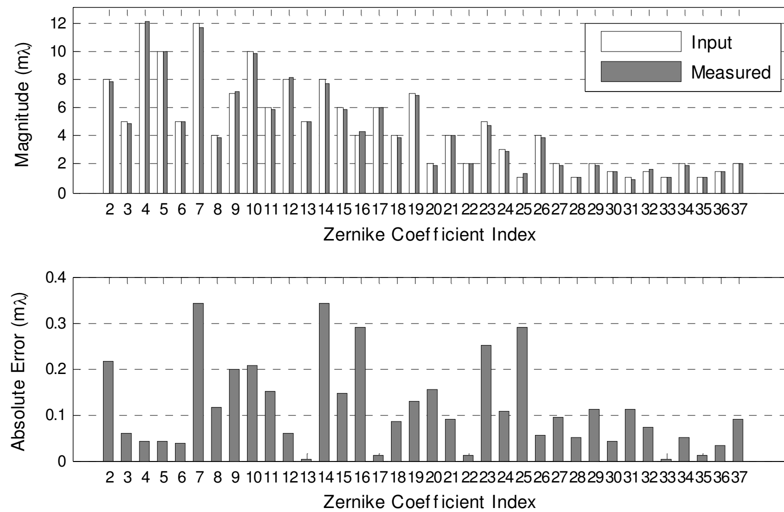

Fig. 8. Simulation result of the proposed technique at partial coherence 0.31 for the Input Aberration 1.

3.3 Accuracy of the proposed technique

To test the accuracy of the proposed technique, all the aberrated wavefronts shown in Fig. 5 were input into the lithographic simulator for the simulated measurements of Zernike coefficient up to Z_{37} at partial coherence 0.31.

Figure 9 shows the simulation result of the measurement errors of individual Zernike coefficients from Z_2 up to Z_{37}. From Fig. 9, all the measurement errors of Zernike coefficients tend to be random distribution and converge in ± 0.4mλ (or ± 0.077nm). Furthermore, the agreement between the input and measured aberrated wavefronts is illustrated in Fig. 10. It is

#111794 - $15.00 USD Received 22 May 2009; revised 31 Jul 2009; accepted 1 Oct 2009; published 9 Oct 2009
(C) 2009 OSA

noted that the absolute measurement errors are less than 3.5mλ (or 0.676nm). The simulation result demonstrates that the proposed technique yields a superior quality of wavefront estimate with an accuracy of Zernike coefficients on the order of 0.1mλs (λ = 193nm) and an accuracy of wavefronts on the order of mλs.

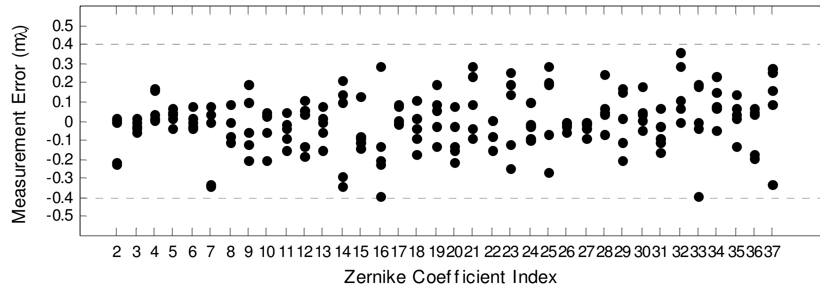

Fig. 9. Simulation result of the measurement errors of Zernike coefficients for all the input aberrated wavefronts.

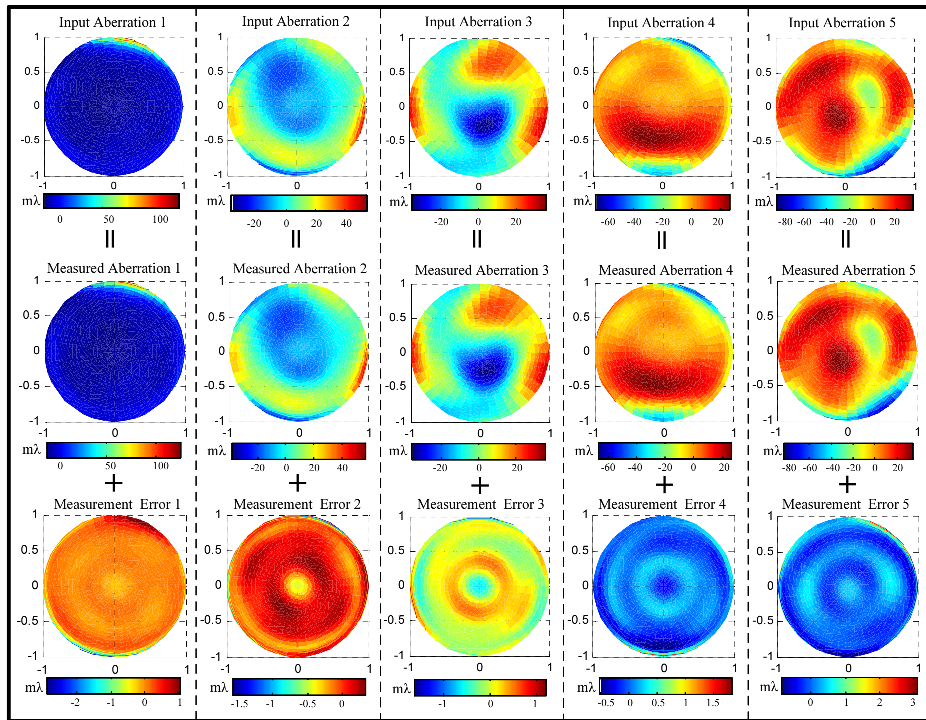

Fig. 10. Agreement between the input and measured aberrated wavefronts.

3.4 Influence of higher-order aberrations

Theoretically lens aberrations should be expressed as the sum of infinite orthogonal Zernike polynomials over the interior of the unit circle. In practice the aberrations are usually expressed as the sum of finite Zernike terms up to Z_N plus a much smaller residual aberration which is the sum of infinite Zernike terms higher than Z_N, where N is the highest concerned order. In our simulation above, all the aberrated wavefronts used as inputs are the sum of Zernike terms from Z_2 to Z_{37}, which indicates that these input aberrations are treated as Zernike terms up to Z_{37} with no residual aberration. These input aberrations can be also

#111794 - $15.00 USD Received 22 May 2009; revised 31 Jul 2009; accepted 1 Oct 2009; published 9 Oct 2009
(C) 2009 OSA

treated as Zernike terms from Z_2 to Z_N (N is less than 37) plus a residual aberration with Zernike terms higher than Z_N. As shown in Fig. 11, for the Input Aberration 5 it is observed that the amount of the residual aberration over the pupil plane corresponding to N = 32 is smaller than that corresponding to N = 25.

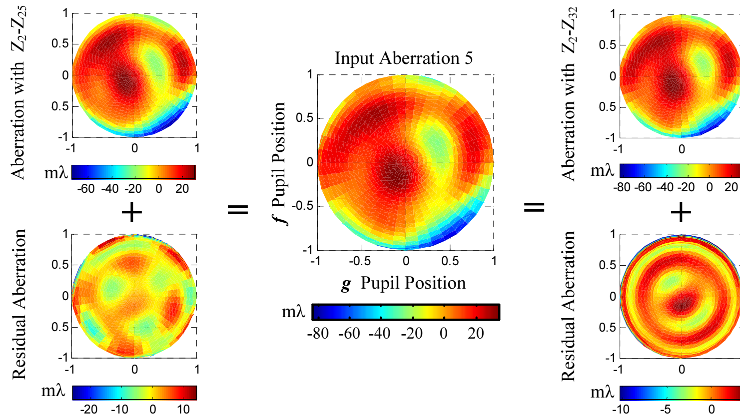

Fig. 11. Different representation of the Input Aberration 5.

To discuss the influence of higher-order aberrations on the performance of our technique, we performed two tests to measure aberrations with Zernike coefficient up to the order N = 25 and N = 32. In this case, each of $\mathbf{Z}_{odd}$ and $\mathbf{Z}_{even}$ in Eqs. (24) and (25) altogether contain N-1 Zernike coefficients. Figure 12 illustrates a direct comparison for each coefficient between the measured results and the input Zernike coefficients. It is clear that the measured Zernike coefficients corresponding to N = 32 match the input coefficients more closely than that corresponding to N = 25, while from Fig. 9 it is noted that the measured results corresponding to N = 37 are in the best correction with the input values. These simulation results reveal that the residual aberration with Zernike terms higher than Z_N has an influence on the measurement of Zernike coefficients from Z_2 to Z_N. Therefore, the aberrations should be measured up to a sufficient high-order Zernike term, so that the unknown residual aberration with high-order Zernike terms could be taken into consideration as possible.

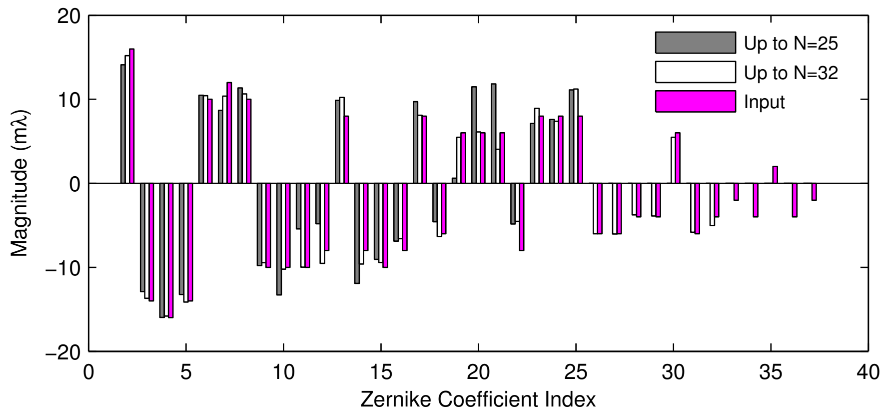

Fig. 12. Measured results of Zernike coefficients up to different orders.

With a set of 36 binary gratings, our proposed technique has been demonstrated to be capable of measuring Zernike coefficient up to the order N = 37. Since the lens aberrations in a real lithographic tool always contain a residual aberration with the order higher than N = 37, it is expected that this higher-order residual aberration will also have an influence on the measurement of Zernike coefficient up to Z_{37}. Fortunately, this influence is little as the

#111794 - $15.00 USD Received 22 May 2009; revised 31 Jul 2009; accepted 1 Oct 2009; published 9 Oct 2009
(C) 2009 OSA

residual aberration with the order higher than N = 37 is usually much small. If there is substantial higher-order residual aberration, the proposed technique can be extended to measure Zernike terms higher than Z_{37} by utilizing a set of gratings with more different pitches and orientations.

4. Conclusion

In this paper, a technique for in situ measurement of lens aberrations up to the 37th Zernike coefficient in lithographic tools has been proposed. Two simplified linear models under partial coherent illumination have been theoretically derived as a compact expression with two matrixes, which relate Zernike coefficients of odd aberration and even aberration respectively to phase shifts and amplitudes of the + 1st-order spectra of aerial image intensities. With the help of the models and using a set of 36 binary gratings with different pitches and orientations, Zernike coefficients for odd aberration and even aberration can be easily determined from the measurement of aerial image intensities.

Although capable of measuring aberrations up to the Z_{37} term, Z37 AIS technique works best under the condition of highly coherent illumination because of obtaining aberrated wavefront at each sampling point. As the partial coherence increases, it has been demonstrated that Z37 AIS technique no longer maintains a high accuracy of wavefront estimate. From the theoretical analysis, the proposed technique has overcome the significant drawback of Z37 AIS technique due to further considering the influence of the partial coherence factor on pupil sampling. Furthermore, the proposed matrixes can be easily calculated in advance by numerical method instead of only by a lithographic simulator, thus lead to improved convenience for aberration measurement.

According to the simulation results, the proposed technique has been proved to be simple in implementation and yield a superior quality of wavefront estimate with an accuracy of Zernike coefficients on the order of 0.1mλs (λ = 193nm) and an accuracy of wavefronts on the order of mλs, and it may hence provide a basis for a practical utility in real-time monitoring of imaging performance of current lithographic tools under partial coherent illumination.

Appendix A: Derivation of Eq. (15)

Consider a very small amount of aberration in the projection lens:

$$\cos\left\{k\left[W_{odd}\left(\alpha_m+f_c,\beta_m+g_c\right)-W_{odd}\left(f_c,g_c\right)\right]\right\}\approx 1, \tag{A-1}$$

$$\cos\left\{k\left[W_{even}\left(\alpha_m+f_c,\beta_m+g_c\right)-W_{even}\left(f_c,g_c\right)\right]\right\}\approx 1, \tag{A-2}$$

$$\begin{aligned}&\arctan\left\{k\iint_{S(\sigma)}\left[W_{odd}\left(\alpha_m+f_c,\beta_m+g_c\right)-W_{odd}\left(f_c,g_c\right)\right]df_c dg_c\right\}\\ &\approx k\iint_{S(\sigma)}\left[W_{odd}\left(\alpha_m+f_c,\beta_m+g_c\right)-W_{odd}\left(f_c,g_c\right)\right]df_c dg_c\ ,\end{aligned} \tag{A-3}$$

$$\sin\left\{k\left[W_{odd}\left(\alpha_m+f_c,\beta_m+g_c\right)-W_{odd}\left(f_c,g_c\right)\right]\right\}\approx k\left[W_{odd}\left(\alpha_m+f_c,\beta_m+g_c\right)-W_{odd}\left(f_c,g_c\right)\right]. \tag{A-4}$$

Substituting Eqs. (A-1) to (A-4) into Eq. (10), the expression of the phase shift of the +1st-order spectrum at the ideal focal plane corresponding to $h = 0$ can be simplified as:

$$\varphi\left(\rho_m,\theta_m,\sigma\right)=k\iint_{S(\sigma)}\left[W_{odd}\left(\alpha_m+f_c,\beta_m+g_c\right)-W_{odd}\left(f_c,g_c\right)\right]df_c dg_c\ . \tag{15}$$

#111794 - $15.00 USD Received 22 May 2009; revised 31 Jul 2009; accepted 1 Oct 2009; published 9 Oct 2009
(C) 2009 OSA

Appendix B: Derivation of Eq. (17)

Consider a very small amount of aberration in the projection lens:

$$\sin\left\{k\left[W_{odd}\left(\alpha_m+f_c,\beta_m+g_c\right)-W_{odd}\left(f_c,g_c\right)\right]\right\}\approx 0, \quad \text{(B-1)}$$

$$\begin{aligned}&\sin\left\{k\left[W_{even}\left(\alpha_m+f_c,\beta_m+g_c\right)-W_{even}\left(f_c,g_c\right)+h\cdot w_{defocus}\left(\alpha_m+f_c,\beta_m+g_c\right)-h\cdot w_{defocus}\left(f_c,g_c\right)\right]\right\}\\&\approx k\left[W_{even}\left(\alpha_m+f_c,\beta_m+g_c\right)-W_{even}\left(f_c,g_c\right)+h\cdot w_{defocus}\left(\alpha_m+f_c,\beta_m+g_c\right)-h\cdot w_{defocus}\left(f_c,g_c\right)\right].\end{aligned} \quad \text{(B-2)}$$

Substituting Eqs. (A-1) and (B-1) into Eq. (11), the amplitude $|I(\rho_m, \theta_m, \sigma, d)|$ of the +1st-order spectrum of aerial image intensity can be simplified as:

$$\begin{aligned}\left|I(\rho_m,\theta_m,\sigma,h)\right|=\frac{1}{(\pi\sigma)^2}\iint_{S(\sigma)}\cos\left\{k\left[W_{even}\left(\alpha_m+f_c,\beta_m+g_c\right)-W_{even}\left(f_c,g_c\right)\right.\right.\\ \left.\left.+h\cdot w_{defocus}\left(\alpha_m+f_c,\beta_m+g_c\right)-h\cdot w_{defocus}\left(f_c,g_c\right)\right]\right\}df_c dg_c.\end{aligned} \quad \text{(B-3)}$$

Substituting Eq. (B-3) into Eq. (16):

$$\begin{aligned}\frac{\partial\left|I(\rho_m,\theta_m,\sigma,h)\right|}{\partial h}=-\frac{k}{(\pi\sigma)^2}\iint_{S(\sigma)}\sin\left\{k\left[W_{even}\left(\alpha_m+f_c,\beta_m+g_c\right)-W_{even}\left(f_c,g_c\right)\right.\right.\\ \left.\left.+h\cdot w_{defocus}\left(\alpha_m+f_c,\beta_m+g_c\right)-h\cdot w_{defocus}\left(f_c,g_c\right)\right]\right\}\\ \times\left[w_{defocus}\left(\alpha_m+f_c,\beta_m+g_c\right)-w_{defocus}\left(f_c,g_c\right)\right]df_c dg_c=0.\end{aligned} \quad \text{(B-4)}$$

Substituting Eq. (B-2) into Eq. (B-4), Eq. (B-4) can be simplified as:

$$\begin{aligned}&\iint_{S(\sigma)}\left[W_{even}\left(\alpha_m+f_c,\beta_m+g_c\right)-W_{even}\left(f_c,g_c\right)+h\cdot w_{defocus}\left(\alpha_m+f_c,\beta_m+g_c\right)-h\cdot w_{defocus}\left(f_c,g_c\right)\right]\\&\times\left[w_{defocus}\left(\alpha_m+f_c,\beta_m+g_c\right)-w_{defocus}\left(f_c,g_c\right)\right]df_c dg_c=0.\end{aligned} \quad \text{(B-5)}$$

From Eq. (B-5), the axial shift $D(\rho_m, \theta_m, \sigma)$ can be obtained by:

$$D(\rho_m,\theta_m,\sigma)=\frac{\begin{aligned}&\iint_{S(\sigma)}\left[W_{even}\left(\alpha_m+f_c,\beta_m+g_c\right)-W_{even}\left(f_c,g_c\right)\right]\\&\times\left[w_{defocus}\left(f_c,g_c\right)-w_{defocus}\left(\alpha_m+f_c,\beta_m+g_c\right)\right]df_c dg_c\end{aligned}}{\iint_{S(\sigma)}\left[w_{defocus}\left(f_c,g_c\right)-w_{defocus}\left(\alpha_m+f_c,\beta_m+g_c\right)\right]^2 df_c dg_c}. \quad (17)$$

Acknowledgments

This work was supported by National Natural Science Foundation of China (Grant No. 50775090), National Basic Research Program of China (Grant No. 2009CB724204), National Hi-Tech Research and Development Program of China (Grant No. 2006AA04Z325), and Program for New Century Excellent Talents in University of China (Grant No. NCET-06-0639). The authors would like to thank National Engineering Research Center for Lithographic Equipment of China for the support of this work and KLA-Tencor Corporation for providing an academic usage product of PROLITH™ software.

#111794 - $15.00 USD Received 22 May 2009; revised 31 Jul 2009; accepted 1 Oct 2009; published 9 Oct 2009
(C) 2009 OSA